Proceedings World Geothermal Congress 2005
Antalya, Turkey, 24-29 April 2005

Numerical Analysis of Transient Behaviours of Geothermal Well Deliverability

Khasani, Ryuichi Itoi and Hikari Fujii

Department of Earth Resources Engineering, Faculty of Engineering, Kyushu University, Fukuoka 812-8581, Japan

E-mail: khasani@mine.kyushu-u.ac.jp

Keywords: well deliverability, transient behaviours, numerical analysis.

ABSTRACT

Deliverability of geothermal production well is evaluated by measuring wellhead pressure versus mass flow rate at several wellhead pressures. Controlling a main valve of the well results in the changes in wellhead pressure and mass flow rate. However, duration required for these variables to stabilize depends on flowing behaviour of steam-water two-phase fluid in the wellbore. The well deliverability is also affected by the reservoir parameters such as reservoir permeability, reservoir pressure and temperature. Thus, transient behaviours of well deliverability were analyzed numerically using a wellbore simulator WELBORE (Miller, 1980). To evaluate the effects of the duration of valve controlling operation on well deliverability, a step change and linear changes with several time intervals in mass flow rate at wellhead were given. The results showed that the duration required for wellhead pressure to stabilize for a given mass flow rate increase in a form of step change is longer compared to that in a form of linear changes. The longer time required for opening valve will result in the faster stabilization of wellhead pressure.

1. INTRODUCTION

In the management of a geothermal resource, careful monitoring of a geothermal reservoir during exploitation is one of the major concerns. This is because fluid extraction from a geothermal reservoir causes a decline in reservoir pressure. This decline of reservoir pressure will lead to changes in surface activities, decrease in well discharge and enhancement of boiling in high-temperature reservoirs. Some of the parameters that need to be monitored include mass discharge of production wells, enthalpy of produced fluid, wellhead pressure, reservoir pressure and temperature.

Deliverability curve that represents the relationship between wellhead pressure and mass flow rate is obtained by measuring both variables for several points by changing a degree of valve opening of the well. During the measurement of well deliverability, time intervals for subsequent measurement of wellhead pressures and flow rates are determined by the experience of operators. However, the duration required for both variables to stabilize depends on various parameters such as reservoir permeability, fluid temperature in the reservoir, and depth of flashing point. Moreover, the duration of valve operation seems to affect the stabilization of well characteristics. Therefore, for a rational design of field measurement of well characteristics, required duration for wellbore to stabilize should be quantitatively evaluated through numerical studies.

There are two methods for measuring steam and water flow rates; (a) lip pressure method and (b) from the well orifice and weir method. In the lip pressure method, the fluid is discharged from the well directly to the atmosphere. The lip pressure is then measured at the extreme end of the discharge pipe using a liquid-filled gauge to damp out pressure fluctuations (Grant *et al*., 1982). In the second method, the orifice is used for steam flow rate discharged from the separator and the weir for the water flow rate leaving from the separator (Lindeburg, 1992). The wellhead pressure is usually measured using a bourdon gauge. Because of the environmental effects, the choice of the measurement using the second method is recommended.

Nakamura *et al*. (1981) presented the deliverability curves of production wells at Takinoue, Japan. Most of the curves indicated the increase in flow rates as the wellhead pressures decrease. The measured flow rates of the steam were in a range of 10 t/h and 130 t/h. The measured pressures and temperatures as well as flashing depth in static and flowing conditions were also measured. However, the duration required for stabilization of flow in a wellbore was not indicated. Fukuda *et al*. (2001) evaluated numerically the pressure profiles at Well O-7 together with its deliverability curve by using a steady state wellbore simulator, at the Otake geothermal field, Japan. The pressure at the feed point decreases with increase in the wellhead pressure.

Itoi *et al*. (1983) studied the change in flow characteristics of a geothermal production well with increasing the drilling depth. The simulated and measured wellhead pressures and flow rates were compared for Hatchobaru production well (H-4) and Otake production well (O-7), Japan. A comprehensive study by Takahashi (1999) described the development of a wellbore flow simulator. The pressure and temperature profiles in wellbore, deliverability curves for measured and calculated results at the wells in Kakkonda geothermal field, Japan was presented. However, the duration between two succeeding measurement of wellhead pressures and flow rates was not considered. Takahashi (1988) also discussed the correlation between flashing depth and wellhead pressure. The importance of knowing the flashing depth is to predict the location for injecting a scale inhibitor into the wellbore when calcite scaling is unavoidable.

Miller (1980) discussed some numerical studies about the transient well deliverability. The studies mainly focus on the transient well test analysis by coupling the wellbore simulator and reservoir model. Wellhead and well bottom pressures under unsteady state due to draw down test were studied.

No research above, however, refer to the duration required for a wellbore flow to stabilize during measurement of wellhead pressures and flow rates induced by controlling wellhead valve. This paper describes the behaviours of well deliverability due to the transient mass flow at the wellhead. The effects of reservoir parameters affecting the well deliverability are also discussed. For this purpose, a reservoir model is incorporated to a wellbore model as well deliverability partly depends on reservoir characteristics.

Thus, a radial flow in a reservoir is considered for an analysis in this study by use of a numerical simulator WELBORE (Miller, 1980).

2. GOVERNING EQUATIONS

The WELBORE simulator was developed on the basis of a set of governing equations both in wellbore and reservoir. Basic equations for fluid flow in the reservoir are derived under assumptions as follows:

1) reservoir is of radial symmetric and horizontal with a constant thickness

2) fluid flow obeys Darcy's law

3) heat exchange between fluid in the wellbore and rock formation is taken into account.

They consist of mass, momentum and energy conservation equations in a vertical wellbore as follows:

Mass:

$$\frac{\partial \rho}{\partial t} + \frac{\partial}{\partial x}(\rho v) = 0 \tag{1}$$

where ρ is the total fluid density (kg/m^3), t is the time (s), x is the spatial distance (m) and v is the fluid velocity (m/s).

Momentum:

$$\frac{\partial}{\partial t}(\rho v) + \frac{\partial}{\partial x}\left[\alpha \rho_s v_s^2 + (1-\alpha)\rho_w v_w^2\right] + \frac{\partial P}{\partial x} + \rho g + \frac{\lambda \rho v^2}{4 r_w} = 0 \tag{2}$$

where α is the void fraction (-), ρ_s is the density of steam (kg/m^3), v_s is the velocity of steam (m/s), ρ_w is the density of water (kg/m^3), v_w is the velocity of water (m/s), P is the pressure (Pa), g is the gravitational acceleration (m/s^2), λ is the friction factor (-), and r_w is the well radius (m). The friction factor λ is evaluated using a two-phase multiplier and is independent of flow regime (Chisholm, 1973).

Energy:

$$\frac{\partial}{\partial t}(\rho e) + \frac{\partial}{\partial x}\left[\alpha \rho_s v_s e_s + (1-\alpha)\rho_w v_w e_w\right] = -P\left\{\frac{\partial}{\partial x}\left[\alpha v_s + (1-\alpha)v_w\right]\right\} + \frac{H}{2 r_w}\left(T - T_{r_w}\right) \tag{3}$$

where e is the specific internal energy of fluid (J/kg), e_s is the specific internal energy of steam (J/kg), e_w is the specific internal energy of water (J/kg), H is the heat transfer coefficient (W/m^2·^{o}C), T is the temperature of fluid in wellbore (^{o}C) and T_{rw} is the temperature of the wellbore wall (^{o}C).

It is required an additional equation of state that correlates between density, pressure and energy of fluids,

$$\Delta \rho = (\partial \rho / \partial P)\Delta P + (\partial \rho / \partial e)\Delta e \tag{4}$$

The reservoir and the wellbore calculations are linked explicitly by using an assumption that the flow rate of mass entering the wellbore is equal to that leaving the reservoir. Pressure changes in time and space in the reservoir is expressed by,

$$\frac{\partial P}{\partial t} = \frac{k}{\mu \varphi C}\left[\frac{\partial^2 P}{\partial r^2} + \frac{1}{r}\frac{\partial P}{\partial r}\right] \tag{5}$$

where k is the permeability (m^2), μ is the dynamic viscosity (Pa·s), φ is the porosity (-), C is the compressibility (1/Pa) and r is the radial distance (m).

Eq. (5) can be expressed further in terms of pressure after discretization as,

$$P_i^{t+1} = P_i^t + \frac{2\Delta t}{(r_{i+1} - r_{i-1})} \cdot \frac{k}{\mu \varphi C} \left[\frac{2}{(r_{i+1} - r_{i-1})}\left(P_{i+1}^t + P_{i-1}^t - 2P_i^t\right) + \frac{1}{r_i}\frac{P_{i+1}^t - P_{i-1}^t}{2}\right] \tag{6}$$

where superscript t denotes the time step and subscript i indicates the nodal point in the radial distance from the wellbore.

3. PROCEDURE OF CALCULATION

Numerical simulations are carried out in the following order,

1) Specify wellbore and reservoir parameters, such as depth of well, well bottom pressure, mass flow rate, specific internal energy of fluid flowing in from the reservoir should be specified and are summarized in Table 1. Furthermore, the properties of the reservoir such as permeability thickness (kh), horizontal extent and storativity (φCh) are also to be given. Other additional parameters are the thermal conductivity of the rock and the thermal diffusivity. A linear temperature profile in the formation of 25^{o}C at the uppermost boundary and 280^{o}C at the bottom boundary is given. The number of grid points in the wellbore is 75, thus the grid length is 13.3 m.

Table 1 Reservoir and Wellbore Parameters

Reservoir	Wellbore
Horizontal Extent : 1500 m	Diameter : 0.2 m
Permeability Thickness : 3 x10^{-12} and 6 x10^{-12} m^3	Length : 1000 m
Storativity : 5x10^{-7} m/Pa$^{*)}$	Roughness : 4.6x10^{-5} m
Thermal Diffusivity : 1x10^{-4} m^2/s $^{*)}$	
Thermal Conductivity : 1.8 W/m/^{o}C$^{*)}$	
Temperature Distribution at Rock Formation : 25^{o}C at the top and 280^{o}C at the bottom	

$^{*)}$ Miller (1980a)

2) Calculate the pressure and temperature profiles in the wellbore and the pressure distribution in the reservoir for initial conditions. The parameters for the initialization consist of well bottom pressure, the specific internal energy of the fluid flowing in from the reservoir and the mass flow rate out of the well.

3) When the stable conditions both in the wellhead and the reservoir are attained, the flow rate at the wellhead is changed to study the transient behaviours of other variables. As the duration required for valve operation seems to affect the transient behaviours of wellhead and well bottom pressures, the mass flow rate at the wellhead is specified as a function of time. The field experience at Hatchobaru showed that the time interval between two subsequent valve operations was set to be about 3 hours (personal communication). The duration for each valve operation was ranging from 5 to 15 mins. To study the effects of the duration of the time interval for mass flow rate change, the time intervals of 0 s (step change), 300 s and 600 s are given and illustrated in Fig. 1. The flow rate is kept constant to be 90 t/h (25 kg/s), then at 600 s it is increased to 180 t/h (50 kg/s) in a different form depending on the time interval for mass flow rate change. The calculation was stopped after 1800 s calculation. At the bottom of the well, the pressure is determined by use of a reservoir model.

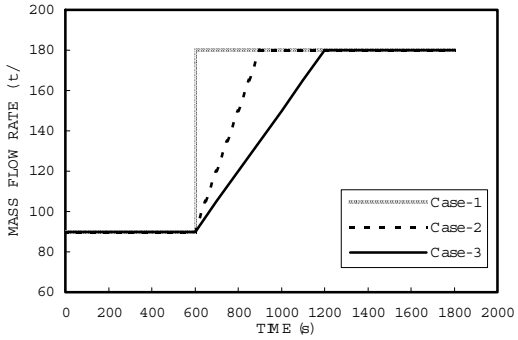

Figure 1: Mass flow rate with time for different time intervals.

4. RESULTS AND DISCUSSION

4.1 The Effects of Time Interval Flow Rate Change on Well Deliverability

Figure 2 shows the changes in wellhead pressure (P_{wh}) with time for three different cases.

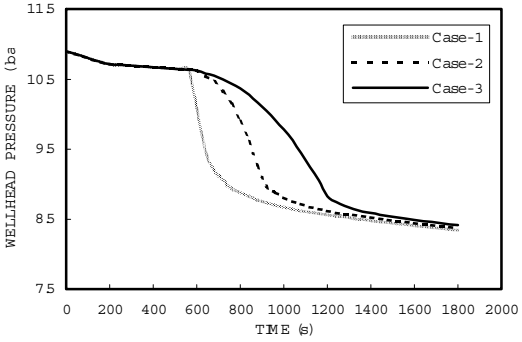

Figure 2: Wellhead pressure (P_{wh}) with time for different time intervals.

Figure 3 shows the simulated results of the well bottom pressure (P_{wb}). The permeability thickness kh = 3 darcy-m is given for these cases. The flow rate change from 90 t/h to 180 t/h is given and the time interval of 0 s (Case-1), 300 s (Case-2) and 600 s (Case-3) are investigated. The P_{wh} for Case-1 quickly drops by 2 bars, and then gradually decreases with time. Other two cases, Case-2 and Case-3, show a smaller decrease in early times, but quickly decrease with time until it reaches to a rather stabilized pressure. The times when decrease rates being moderated correspond to those when flow rate reach to 180 t/h. On the other hand, P_{wb} for all cases show decrease with time and their decrease rates seem to be reflected by a mode of flow rate change (Fig. 1).

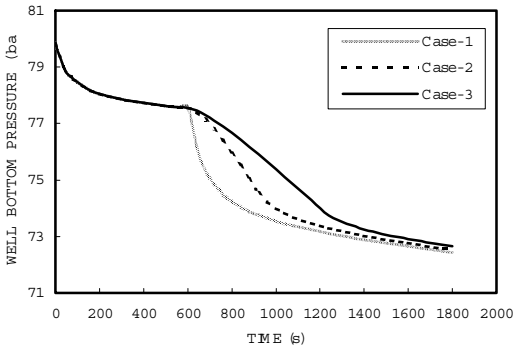

Figure 3: Well bottom pressure (P_{wb}) changes with time for different time intervals.

The transient behaviours of P_{wh} and P_{wb} are analysed by evaluating Eqs. (1) to (3). By combining these equations, the pressure distribution in the wellbore can be calculated. Pressure drop in a well consists of pressure drops due to potential, acceleration and friction. Figure 4 compares the pressure drop components at the wellhead for Case-1.

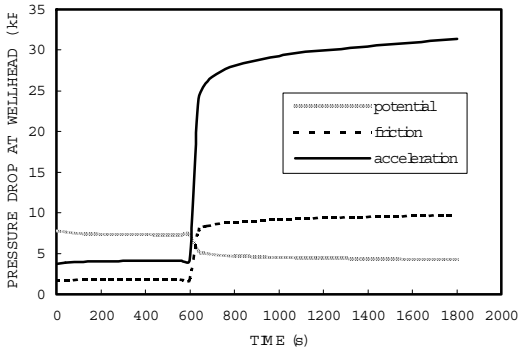

Figure 4: Pressure drop component at wellhead with time.

For the low flow rate under stable condition up to 600 s, the pressure drop is dominated by potential component. The increase in the mass flow rate from 90 t/h to 180 t/h at 600 s is followed by the increase in pressure drops for friction and acceleration components. On the other hand, the pressure drops due to potential component decreases. This suggests that the increase in flow rate leads to an increase of fluid velocity mainly along two-phase flow region, then resulted in more pressure drop due to acceleration. The changes both in average density and velocity of two-phase fluid at wellhead are shown in Fig. 5. At low flow rate, the density of the fluid is higher than that of higher flow rate after 600 s. On the other hand, the velocity of the fluid increases after changing the mass flow rate at 600 s. This velocity and density change behaviour is the reason why the pressure drop at low flow rate is dominated by potential component rather than acceleration one where the fluid velocity of water single-phase is low. While for the higher flow rate, the pressure drop is dominated by acceleration component due to the high fluid velocity.

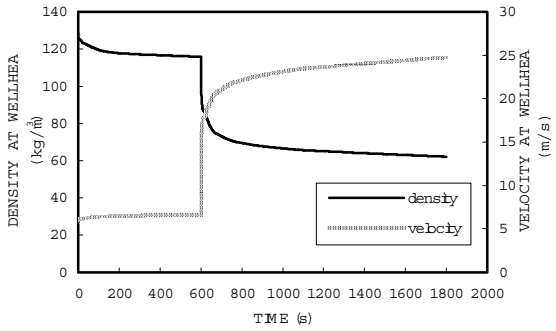

Figure 5: Fluid density and velocity at wellhead with time.

4.2 The Effects of Permeability Thickness (*kh*)

4.2.1 On Wellhead and Well Bottom Pressures

The effects of *kh* on P_{wh} and P_{wb} are illustrated in Figs. 6 and 7 for Case-1 and Case-3, respectively. Two values of *kh*, 3 darcy-m and 6 darcy-m are given, based on the measured data at Hachobaru field (Tokita *et al.*, 2002). At the early times, both P_{wh} and P_{wb} decrease with time and show small decrease as the time elapses. After an increase in the flow rate from 90 t/h to 180 t/h at 600 s for both Case-1 and Case-3, P_{wh} and P_{wb} decrease with time and require different time to stabilize. The duration of time required for changing the flow rate (Case-1 and Case-3) give similar values for both P_{wh} and P_{wb}. For Case-1, the change in flow rate causes the P_{wh} decrease sharply. Then P_{wh} gradually decreases and stabilizes. On the other hand, for Case-3, the change in flow rate results in a decrease in P_{wh} at the beginning and the decrease rate becomes larger as the time elapses. Then, as soon as the higher flow rate has been reached at 1200 s the P_{wh} shows a small decrease and reaches stable value. It can be seen that the time required for P_{wh} to stabilize is shorter for Case-3 compared to that for Case-1. Quick decrease in P_{wb} can also be seen for Case-1 then followed by a smaller decrease as time elapses. While for Case-3, P_{wb} linearly decreases with time. The stabilization between Case-1 and Case-3 for low *kh* = 3 darcy-m (solid lines) is faster than those of high *kh* = 6 darcy-m (dashed lines).

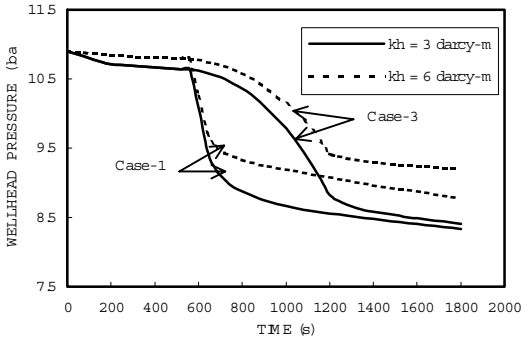

Figure 6: Wellhead pressure vs time for different *kh*.

After increase in the flow rate, both P_{wh} and P_{wb} are low for small *kh* for both Case-1 and Case-3. To explain this situation, we may evaluate two different points; first is one at the low flow rate condition and the second is at higher flow rate. If the reservoir flow can be assumed to be under steady state when the flow rate of the well reaches to stable condition, the steady state equation with respect to Eq. (5) can be applied. Thus the flow rate in the wellbore can be expressed by specifying boundary conditions as,

$$r = r_w \qquad p = P_{wb}$$

$$r = r_e \qquad p = P_e$$

then,

$$G = \frac{2\pi kh\rho_w (P_e - P_{wb})}{\mu_w R_e} \tag{8}$$

where μ_w is the dynamic viscosity of water (Pa·s), and ρ_w is the water density (kg/m^3). As μ_w and ρ_w are assumed to be constant in the reservoir the flow rate depends only on *kh* and P_{wb}.

For a given flow rate (180 t/h), an increase in *kh* will result in the decrease in ($P_e - P_{wb}$). Thus, P_{wb} must increase. That is why, P_{wb} for *kh* = 6 darcy-m is always higher than that for *kh* = 3 darcy-m.

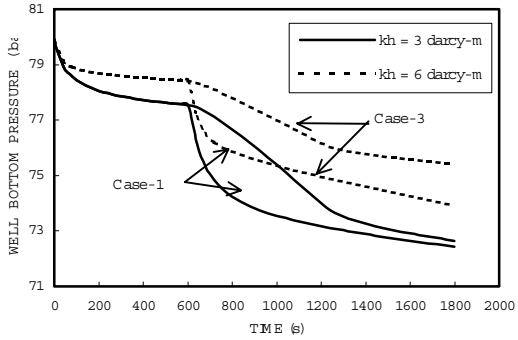

Figure 7: Well bottom pressure vs time for different *kh*.

4.2.2 On Flashing Depth

Flashing depth is a point where the liquid hot water starts to generate steam. The flashing starts when the pressure reaches the saturation pressure corresponding to the fluid temperature at depth. Figure 8 represents the flashing depth with time for different *kh* of Case-3. Flashing depths locate at a depth of 267 m for both *kh* = 3 darcy-m and *kh* = 6 darcy-m, respectively at first, then they go downward as flow rate at wellhead is kept constant at 90 t/h up to 600s and changed linearly to 180 t/h in the period from 600 s to 1200 s. From thermodynamic point of view, the flashing point depends on the pressure and the temperature of the fluid at the feed zone. In this study the fluid phase entering the wellbore always in the liquid form, so the temperature of the fluid at the feed zone can be treated constant. Therefore, the change in the flashing depth for different *kh* is mainly due to P_{wb}. The flashing depth for *kh* = 3 darcy-m locates at 267 m depth from the beginning of the calculation and decreases to 305 m at 600 s. While it locates at a depth of 267 m and decreases at 290 m for *kh* = 6 darcy-m. This corresponds to the P_{wb} at 77.5 bar for *kh* = 3 darcy-m and at 78.5 bar for *kh* = 6 darcy-m. The changes of the flashing depth with time also depend on the *kh*. This is because the decrease rate of the P_{wb} is dependent on *kh*. The decrease rate of the P_{wb} is higher for the lower *kh*. As the result, the decrease rate in the flashing depth is also higher for lower *kh*. For *kh* = 3 darcy-m case, the decrease in P_{wb} of 6 bar from the beginning to 1200 s causes the flashing depth moves downwards at about 70 m. While for *kh* = 6 darcy-m one, the P_{wb} drop of 3.8 bar leads to a flashing depth change of 43 m.

Figure 9 shows the pressure profiles in the wellbore at different elapsed time for *kh* = 3 darcy-m (a) and *kh* = 6 darcy-m (b).

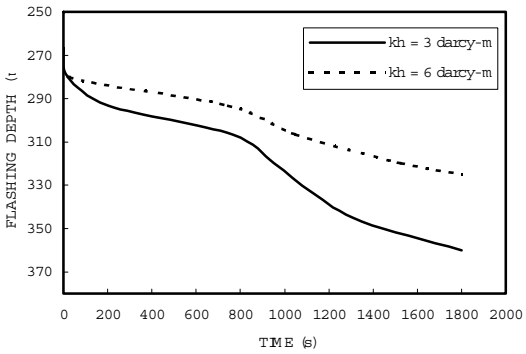

Figure 8: Flashing depth vs time for different *kh*.

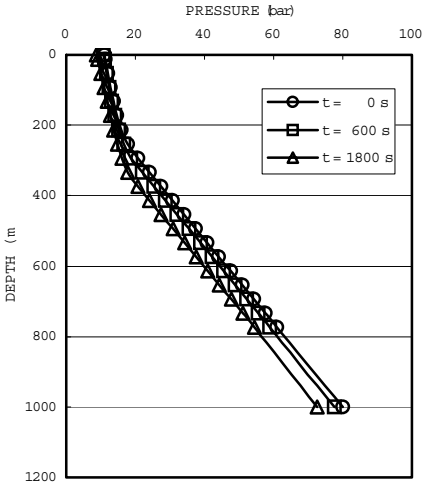

(a) *kh* = 3 darcy-m

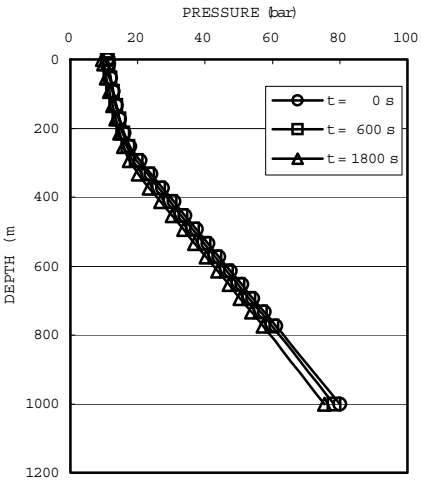

(b) *kh* = 6 darcy-m

Figure 9: Pressure profiles at different elapsed time for different *kh*.

From 600 s to 1800 s, the decrease in P_{wb} by 5 bar causes P_{wh} drop by 2.2 bar for *kh* = 3 darcy-m. On the other hand, for *kh* = 6 darcy-m the P_{wb} and P_{wh} drops by 3 and 1.6 bar, respectively are observed. The decrease in P_{wb} due to the increase in the flow rate causes the flashing point move downwards. Comparison between these calculated results and the measured data presented by Nakamura (1981) show that a relatively similar behavoiurs for the parameters has been observed. The measured pressure profiles together with corresponding mass flow rates and flashing depth were presented. The flow rates of 78 t/h, 148 t/h and 200 t/h correspond to the P_{wh} at 12 bar, 10.9 bar and 10 bar and flashing depths at about 352 m, 470 m and 560 m, respectively. The measured P_{wb} were 76 bar, 64 bar and 57 bar. The difference between the measured data and the calculated result is due to the difference in geometry of the wellbore, reservoir properties and given flow rates.

4.3 The Effects of Permeability Thickness (*kh*) Heterogeneity

To evaluate the effects of the permeability changes of a zone surrounding the well either increase or decrease in *kh* numerically on well characteristics and reservoir pressure, the term "skin" that usually appears in the line source solution is used. In this study the term "skin" is defined as follow (Horne, 1995),

$$s = \left(\frac{k}{k_s} - 1\right) \ln \frac{r_s}{r_w} \tag{9}$$

where k is the permeability (m^2), k_s is the skin zone permeability (m^2), r_s is the damaged/stimulated zone radius (m) and r_w is the wellbore radius (m).

The procedure of the evaluation is carried out as follows,

1) Define the damaged/stimulated zone radius, r_s

2) Estimate the skin zone permeability, k_s for damaged/stimulated cases

3) The value of s can be calculated using Eq. (9) and it may be positive or negative

4) The values of r_s and k_s then are given as input data for the program.

Two values of skin effects, 5 and –5, are evaluated. This corresponds to decrease and increase permeability thickness of 1.1×10^{-12} darcy-m and 4.6×10^{-12} darcy-m, respectively from the homogeneous permeability of the reservoir of 3×10^{-12} darcy-m. The damaged/stimulated zone radius, r_s is assumed to be 2 m. Figures 10 and 11 show the P_{wh} and P_{wb} changes with time for conditions with and without skin. Similar behaviours can be observed for both parameters. For positive skin (s=5), the P_{wh} and P_{wb} are always lower than those without skin. The difference for P_{wh} and P_{wb} between positive skin and without skin becomes large as the time elapses. In contrast, for negative skin (-5) the P_{wh} and P_{wb} are always higher than those without skin. It can be noted that even the magnitude of the skin value is the same, the positive skin gives larger pressure drop than the negative skin that causes smaller increase in both P_{wh} and P_{wb}.

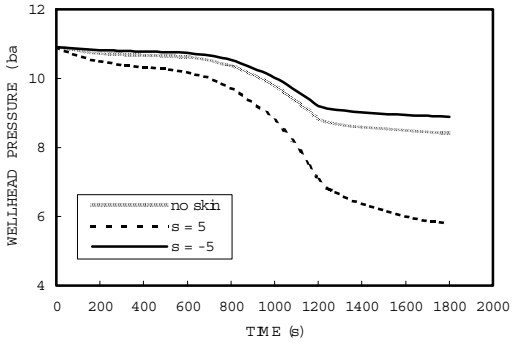

Figure 10: Effects of skin on wellhead pressure change with time.

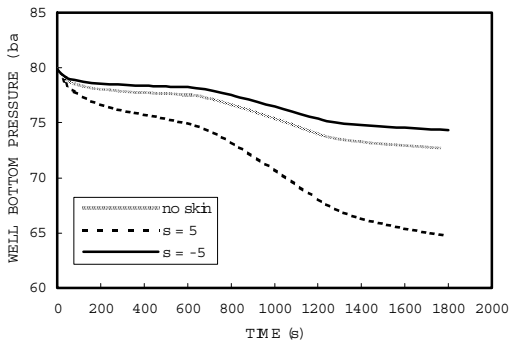

Figure 11: Effects of skin on well bottom pressure change with time.

Figure 12 illustrates the reservoir pressure distributions for conditions described above. The reservoir distributions are taken for the calculated times of 0.5 s and 1800 s. It can be seen that at the beginning (0.5 s) all reservoir pressure distributions are almost the same. While significant changes after 1800s can be observed, especially for the pressure distributions at the zone close to the wellbore at a distance of less than 10 m. It can be clearly seen that at the distance of about 2 m close to the wellbore where the changes in permeability are found, the reservoir pressure distributions show the decrease for positive skin and increase for negative skin compared to the condition without skin.

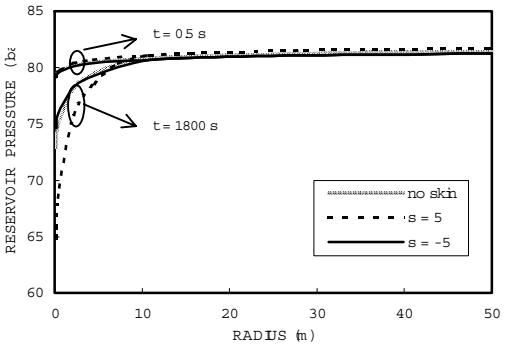

Figure 12: Effects of skin on reservoir pressure.

5. CONCLUSIONS

From the above analyses of the results, the following conclusions have been drawn:

The numerical simulation for a given wellbore and reservoir condition shows that the step change and short period of time interval change in flow rate produces a sharp decrease in wellhead pressure. While longer time interval changes in flow rate show gradual decreases.

The time required for the wellhead pressure and the well bottom pressure to stabilize is reached faster for longer time interval change in the flow rate.

The lower *kh* results in higher well bottom pressure at lower flow rate condition, while it gives lower values for higher flow rate condition. The changes of the fluid density in the well bottom with time seem to attribute this phenomenon.

The higher *kh* will produce smaller movement of the flashing depth for the same flow rate condition. The decrease rate of the flashing depth is higher for lower *kh*.

The numerical study of the skin effects by using coupled wellbore and reservoir model is possible, but it needs to be verified with the analytical solution.

ACKNOWLEDGEMENTS

The first author gratefully acknowledges the scholarship by the Ministry of Education, Culture, Sports, Science and Technology, Government of Japan.

REFERENCES

Chisholm, D.: Pressure Gradients Due to Friction during the Flow of Evaporating Two-Phase Mixtures in Smoother Tubes and Channels, *International Journal Heat Mass Transfer*, **16**, (1973), 347-358.

Fukuda, M., Nakamura, H., Matsuura, S., Tanaka, T., and Itoi, R.: An Analysis of Steam-Water Two-Phase Flow in the Geothermal Well, *Proceedings*, 22nd Annual PNOC-EDC Geothermal Conference, March 13-14, (2001).

Grant, M. A., Donaldson, I. G. and Bixley, P. F.: Geothermal Reservoir Engineering. *Academic Press.* (1982).

Horne, R. N. : Modern Well Test Analysis. A Computer-Aided Approach. 2nd Edition. Petroway, Inc. (1995), 257p.

Itoi, R., Fukuda, M., Sekoguchi, K., and Iwaki, T.: Theoretical Study on Steam and Water Flow Rates from Geothermal Production Wells. *Journal of Geothermal Research Society of Japan*, **5**, No.4, (1983), 235-248.

Lindeburg, M. R.: Engineer-In-Training Reference Manual. 8th Edition. *Professional Publications, Inc.* (1992).

Miller, C. W.: *Welbore User's Manual*, Lawrence Berkeley Laboratory, University of California, (1980a), 48p.

Miller, C. W.: Eliminating the Wellbore Response in Transient Well Test Analysis. *Proceedings*, 6th Workshop on Geothermal Reservoir Engineering, Stanford, CA, (1980b).

Nakamura, H. and Kiyoshi, S.: Exploration and Development at Takinoue, Japan, *In: Geothermal Systems: Principles and Case Histories*. Ed: L. Rybach and L.J.P. Muffler, John Wiley & Sons Ltd., (1981), 247-272.

Takahashi, M.: A Wellbore Flow Model in the Presence of CO_2 Gas. *Proceedings*, 13th Stanford Geothermal Workshop, Stanford University, CA, (1988).

Takahashi, M.: Development of a Wellbore Flow Simulator (WELCARD-III). *Journal of Geothermal Research Society of Japan*, **21**, No.1, (1999), 13-28.

Takahashi, M.: Development of a Wellbore Flow Simulator (WELCARD-IV). *Journal of Geothermal Research Society of Japan*, **21**, No.2, (1999), 115-126.

Takahashi, M.: Development of a Wellbore Flow Simulator (WELCARD-IV). *Journal of Geothermal Research Society of Japan*, **21**, No.2, (1999), 115-126.

Tokita, H., Momita, M., and Koide, K.: A Rough Estimation of Deep Geothermal Potentials of the Hohi and Ogiri Areas, Japan with Simplified Numerical Model. *Proceedings*, 23rd Annual PNOC-EDC Geothermal Conference, Makati City, Philippines, (2002).